

# The Matter Radius of $^{132}\text{Sn}$ and the CREX–PREX Dilemma

J. Piekarewicz<sup>1</sup>

<sup>1</sup>*Department of Physics, Florida State University, Tallahassee, FL 32306, USA*

(Dated: March 13, 2026)

The density dependence of the nuclear symmetry energy remains a central open problem in nuclear physics. Parity violating electron scattering experiments have provided largely model-independent determinations of the neutron skin thickness of both  $^{48}\text{Ca}$  and  $^{208}\text{Pb}$ , whose consistent theoretical interpretation remains challenging. A new measurement of the matter radius of the unstable, doubly magic nucleus  $^{132}\text{Sn}$  provides an important additional constraint. Using a representative set of covariant energy density functionals spanning a wide range of isovector properties, we show that at least one of these models can simultaneously reproduce the charge and matter radii of  $^{132}\text{Sn}$ . When interpreted together with the PREX and CREX results, the new measurement—much like CREX—favors a relatively soft symmetry energy. These findings underscore the need for an independent confirmation of the PREX result, such as the anticipated MREX campaign at the MESA facility.

The density dependence of the nuclear symmetry energy remains one of the central open questions in nuclear science, with profound implications for both neutron-rich nuclei and neutron stars; see Refs.[1–5] and references contained therein.

Specifically, parity violating electron scattering experiments on both  $^{208}\text{Pb}$  (PREX) [6–8] and  $^{48}\text{Ca}$  (CREX) [9] at the Thomas Jefferson National Accelerator Facility have provided the first model-independent determinations of the weak form factor at precisely selected momentum transfers. Parity-violating scattering is uniquely powerful because it avoids the strong-interaction uncertainties inherent in hadronic measurements. While the transition from the weak form factor to the neutron radius—and the resulting neutron skin thickness—is mildly model dependent [8], these measurements currently offer the cleanest determination of the neutron radii of  $^{48}\text{Ca}$  and  $^{208}\text{Pb}$ .

Unfortunately, a combined interpretation of these results has proven to be remarkably challenging. While PREX favors a relatively thick neutron skin in  $^{208}\text{Pb}$  that is consistent with a stiff symmetry energy [8, 10], CREX measured a significantly thinner skin in  $^{48}\text{Ca}$  [9], suggesting a softer symmetry energy near saturation density. Reconciling these seemingly contradictory findings within a unified theoretical framework has exposed significant tensions in both density functional theory and ab initio approaches [11–26].

In this context, the recent experimental extraction of the matter radius of the doubly magic nucleus  $^{132}\text{Sn}$  provides a critical new benchmark [27]. For decades  $^{132}\text{Sn}$ —with closed shells of 50 protons and 82 neutrons, and a lifetime of nearly 40 seconds—has been a cornerstone of nuclear physics due to its robust “doubly magic” character [28, 29]. Because of its structural simplicity,  $^{132}\text{Sn}$  has long served as an ideal testing ground for theoretical models [11, 30] and the investigation of exotic collective modes sensitive to the nuclear symmetry energy [31–37].

Detailed structural information on  $^{132}\text{Sn}$  began to emerge in 2005 with a precise measurement of its charge radius. Laser spectroscopy studies of neutron-rich tin isotopes performed at the ISOLDE facility yielded a precisely measured charge radius of  $R_{\text{ch}}^{132} = 4.709(7)$  fm [38]. Soon thereafter, reactions on nuclei neighboring  $^{132}\text{Sn}$  provided direct access to single-particle states outside the  $N = 82$  shell closure [39, 40]. These

experiments showed that the spectroscopic strength associated with the valence neutron orbitals is consistent with a pronounced shell closure, thereby reinforcing the magic nature of  $^{132}\text{Sn}$ .

Beyond nuclear structure,  $^{132}\text{Sn}$  also plays an important role in nucleosynthesis, as it lies close to the path of the r-process responsible for producing roughly half of the heavy elements [39, 41]. Taken together, these experimental advances have strongly influenced theoretical developments. A unified description of the single-particle spectrum, the charge radius, and now the matter radius is essential for developing a comprehensive picture of how neutrons and protons are distributed within the short-lived, neutron-rich nucleus  $^{132}\text{Sn}$ .

With an isospin asymmetry even larger than that of  $^{208}\text{Pb}$ ,  $^{132}\text{Sn}$  offers enhanced sensitivity to isovector dynamics while remaining amenable to both density functional theory and ab initio calculations [11, 30]. The measured matter radius,  $R_{\text{m}}^{132} = 4.758^{+0.023}_{-0.024}$  fm, when combined with the charge radius points—much as in the case of  $^{48}\text{Ca}$ —to a relatively thin neutron skin. As relevant, Hijikata and collaborators concluded that “there are no theoretical calculations consistent with both matter and charge radii within the experimental errors” [27]. Hence, any realistic description of the nuclear symmetry energy must now account not only for the neutron skins of  $^{48}\text{Ca}$  and  $^{208}\text{Pb}$ , but also for the correlated charge-matter radius systematics emerging in  $^{132}\text{Sn}$ . The delicate interplay among these nuclei therefore provides a uniquely stringent test of modern energy density functionals and ab initio approaches. The combined constraints from  $^{48}\text{Ca}$ ,  $^{132}\text{Sn}$ , and  $^{208}\text{Pb}$  thus define a powerful triplet of doubly-magic nuclei that sharpens our understanding of isovector dynamics and of the density dependence of the symmetry energy.

The results presented in this letter were obtained within a covariant framework based on a Lagrangian density written in terms of nucleon, photon, and three meson fields that mediate the nuclear interaction. The structure of the Lagrangian density has been documented extensively in earlier publications [42], while details of the specific models employed in this work may be found in Refs.[43–45].

In Fig.1 we display predictions for the probability distribution functions of the charge and matter radii of  $^{132}\text{Sn}$  as obtained with FSUGarnet—a covariant energy density func-

tional introduced in Ref.[45]. The distributions were generated from 10,000 configurations sampled according to the covariance matrix obtained from the optimization of the functional. The circles represent the histogram, while the solid curve denotes the associated Gaussian fit. Also shown are the experimental values for the charge [38] and matter radii [27]. Contrary to the assertion by Hijikata *et al.*, theoretical calculations exist that are consistent with both the measured charge and matter radii. As we elaborate below, the real challenge for the theoretical community is to reconcile all the existing measurements, namely, PREX, CREX and now the RIKEN results.

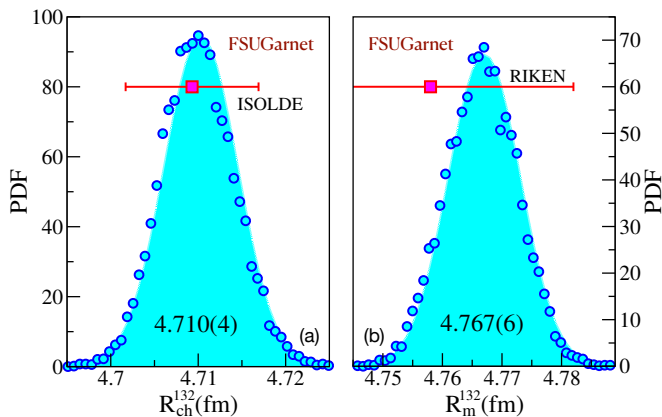


FIG. 1. Theoretical predictions for the charge and matter radii of  $^{132}\text{Sn}$ . The probability distribution functions were generated with FSUGarnet [45] and the experimental data are from ISOLDE [38] and RIKEN [27], respectively.

Together with the charge and matter radii displayed in Fig.1, we now list in Table I the charge, matter, neutron, and neutron skin radii of  $^{132}\text{Sn}$  as predicted by three representative covariant energy density functionals: FSUGarnet, RMF022, and FSUGold2 [44, 45]. That all three models agree on their predictions for the charge radii is not surprising, given that the charge radius of  $^{132}\text{Sn}$  was incorporated into the calibration of the functionals. Note that the charge radius was defined in the calibration of the various functionals simply as  $R_{\text{ch}}^2 = R_p^2 + r_{\text{ch}}^2$ , where  $R_p$  is the point proton radius and  $r_{\text{ch}} = 0.88$  fm is the single-proton charge radius—an adopted value that is slightly larger than the current CODATA value of  $r_{\text{ch}} = 0.84$  fm. The models primarily disagree in the calibration of the isovector sector: FSUGarnet predicts the softest symmetry energy and the thinnest neutron skin, while in turn, FSUGold2 predicts the stiffest symmetry energy and the thickest neutron skin. Note that a “soft” or “stiff” symmetry energy refers to the slope parameter of the symmetry energy at saturation density ( $L$ ), a quantity that correlates strongly with the value of the neutron skin thickness of heavy nuclei [46–48]. The slope of the symmetry energy for the functionals selected in this work are:  $L = 50.96, 63.52, 112.84$  MeV, for FSUGarnet, RMF022, and FSUGold2, respectively.

Model	$R_{\text{ch}}$ (fm)	$R_{\text{m}}$ (fm)	$R_{\text{n}}$ (fm)	$R_{\text{skin}}$ (fm)
FSUGarnet	4.710(4)	4.767(6)	4.850(10)	0.223(12)
RMF022	4.706(4)	4.799(7)	4.904(11)	0.280(13)
FSUGold2	4.707(5)	4.846(13)	4.976(19)	0.352(16)
Experiment	4.709(7)	4.758(24)	4.824(38)	0.178(39)

TABLE I. Predictions for the charge, matter, neutron, and neutron-skin radii of  $^{132}\text{Sn}$  obtained with the three covariant energy density functionals employed in this work. The uncertainties in the experimental neutron radius and neutron skin thickness were obtained via standard error propagation.

Although charge radii are fundamental observables for the calibration of energy density functionals, a more stringent test of the theoretical framework is provided by the corresponding densities and form factors. To place the discussion in the proper context, we highlight several useful properties of the “symmetrized” two-parameter Fermi function. Although it is practically indistinguishable from the standard two-parameter Fermi (2pF) form when the half-density radius  $c$  is much larger than the surface diffuseness  $a$ , the symmetrized version exhibits significantly improved analytic properties [49]. Starting from the conventional 2pF distribution, the symmetrized form may be written as follows:

$$f_{\text{SF}}(r) \equiv f_{\text{F}}(r) + [f_{\text{F}}(-r) - 1] = \frac{\sinh(c/a)}{\cosh(r/a) + \cosh(c/a)}. \quad (1)$$

A particularly attractive feature of the symmetrized Fermi function is that—unlike the conventional 2pF function—its form factor can be computed analytically [49]. Consequently, all spatial moments of the distribution may be computed exactly. In particular, at low momentum transfers, the form factor admits the Taylor expansion

$$F_{\text{SF}}(q) = 1 - \frac{q^2}{3!}R^2 + \frac{q^4}{5!}R^4 + \dots \quad (2)$$

where the first two moments are given by [50]

$$R^2 \equiv \langle r^2 \rangle = \frac{3}{5}c^2 + \frac{7}{5}(\pi a)^2, \quad (3a)$$

$$R^4 \equiv \langle r^4 \rangle = \frac{3}{7}c^4 + \frac{18}{7}(\pi a)^2 c^2 + \frac{31}{7}(\pi a)^4. \quad (3b)$$

This expansion highlights the intimate connection between the low- $q$  behavior of the form factor and the spatial moments of the underlying density distribution, with the leading correction determined by the mean-square radius. Thus, measurements of the form factor at sufficiently small momentum transfers provide direct access to the rms radius of the nucleus.

Now displayed in Fig.2(a) are proton, neutron, and matter densities as predicted by the three covariant energy density functionals listed in Table I. Although agreement on charge radii does not guarantee consistency across the entire spatial density, we observe that all three models predict nearly identical proton distributions. This consistency, however, does not extend to the neutron or matter densities. The long-standing hope has been that experimental measurements could

resolve these differences and thereby constrain the density dependence of the symmetry energy. Yet experimental two-parameter Fermi (2pF) distributions are—by construction—flat in the nuclear interior and therefore incapable of resolving the detailed internal structure of the nucleus. This reflects a generic feature of elastic scattering with strongly interacting probes, which are primarily sensitive to the nuclear surface.

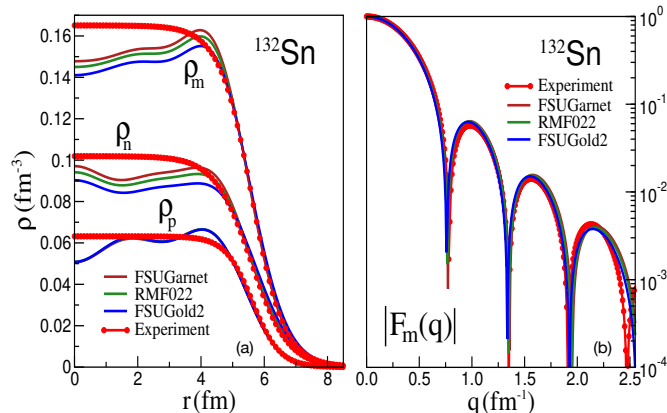


FIG. 2. (a) Proton, neutron, and matter densities of  $^{132}\text{Sn}$  predicted by the three covariant energy density functionals used in this work, together with densities extracted from experiment using two-parameter Fermi distributions. (b) Corresponding matter form factors. Because protons probe primarily the nuclear surface, model differences appear only at large momentum transfer, where the form factor has already fallen by more than two orders of magnitude.

The matter form factor, obtained from the Fourier transform of the spatial densities shown in Fig.2(b), reinforces this picture. Given the surface dominance of the probe, the matter form factor is largely insensitive to any model dependence. Differences between the models and the experimental 2pF form factor do not emerge until the fourth diffraction maximum, by which point the form factor has already decreased by more than two orders of magnitude. Although model differences in the neutron skin thickness are predicted to be as large as 60%, the corresponding differences in the matter radius remain below 2%. Because the characteristic diffractive oscillations of the elastic cross section are governed primarily by the matter radius, the large spread in neutron skin predictions among the various models becomes greatly diluted [51]. Listed in Table II are the two-parameter symmetrized Fermi distributions for the proton and neutron densities of  $^{132}\text{Sn}$  as predicted by the three covariant energy density functionals considered in this work, together with those extracted from experiment; see Table 3 of Ref.[27]. A notable difference between the theoretical predictions and the experimental extraction is that, in all the theoretical models, the neutron half-density radius is consistently larger than the corresponding proton radius.

Model	$c_p$	$a_p$	$R_p$	$c_n$	$a_n$	$R_n$
FSUGarnet	5.637	0.412	4.627	5.709	0.536	4.850
RMF022	5.631	0.412	4.623	5.771	0.542	4.903
FSUGold2	5.630	0.415	4.626	5.867	0.545	4.976
Experiment	5.632	0.430	4.646	5.581	0.576	4.824

TABLE II. Two-parameter symmetrized Fermi distributions for the proton and neutron densities—and the corresponding radii—of  $^{132}\text{Sn}$  predicted by the three covariant energy density functionals employed in this work. For the experimentally extracted parameters, we list the central values reported in Table 3 of Ref.[27]. All quantities are given in fm.

As we continue to explore the era of rare-isotope beams, it is therefore important to determine whether hadronic probes—despite their surface sensitivity—can be refined to provide meaningful constraints on the neutron skins of exotic nuclei with large neutron excess. This question is especially relevant given that the model-independence of parity-violating electron scattering is experimentally unattainable for unstable nuclei. Nevertheless, the PREX and CREX measurements provide valuable anchors for guiding new hadronic experiments and constraining theoretical models.

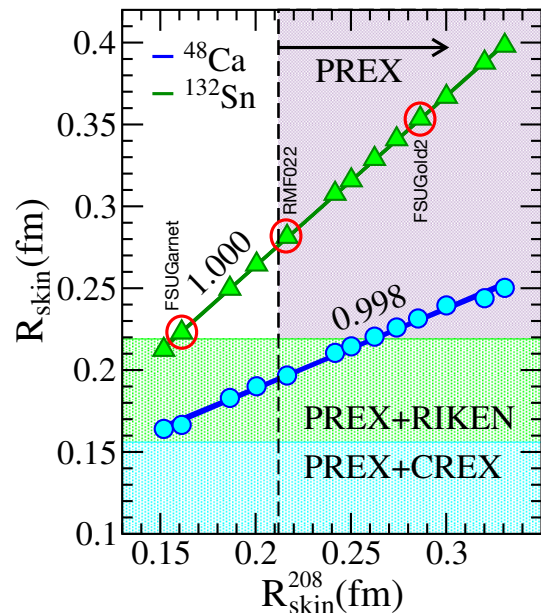


FIG. 3. Predicted correlation between the neutron skin thickness of  $^{208}\text{Pb}$ ,  $^{132}\text{Sn}$ , and  $^{48}\text{Ca}$  from a set of covariant energy density functionals. The PREX, CREX, and RIKEN constraints are also shown. Indicated with red circles are the predictions from FSUGarnet, RMF022, and FSUGold2. The tight correlation illustrates the challenge of reconciling the neutron skins of these three nuclei within a single theoretical description.

The challenge of extracting the neutron skin from surface-dominated hadronic probes becomes even more pressing

when considering the current ‘‘CREX–PREX dilemma’’. As noted earlier, the challenge is not to reproduce the charge and matter radius of  $^{132}\text{Sn}$ , but rather to do so in the context of the CREX–PREX tension. Whereas FSUGold2 is distinctly ‘‘PREX-like’’ in its prediction of a stiff symmetry energy and a thick neutron skin, FSUGarnet is ‘‘CREX-like,’’ favoring a significantly softer symmetry energy and correspondingly thinner neutron skin—highlighting a potential deficiency in the current generation of energy density functionals. The inclusion of the RMF022 functional serves as an intermediate case between the soft FSUGarnet and stiff FSUGold2.

As a neutron-rich, doubly magic nucleus,  $^{132}\text{Sn}$  offers a unique bridge: if proton scattering in inverse kinematics can provide a reliable skin thickness for this isotope, it may clarify the PREX–CREX discrepancy and offer a path forward in the determination of the equation of state. The hope is that a single functional can consistently describe the evolution of the neutron skin across the nuclear chart. The problem with this scenario is that the neutron skin thickness of  $^{208}\text{Pb}$ ,  $^{132}\text{Sn}$ , and  $^{48}\text{Ca}$  are highly correlated, so it is challenging to reproduce all with current energy density functionals. In Fig.3 we display such a correlation using 13 covariant energy density functionals of the kind used in this work. Whereas the CREX-like FSUGarnet functional is almost consistent with the CREX and RIKEN results, its predictions for the neutron skin thickness of  $^{208}\text{Pb}$  is inconsistent with PREX. Conversely, FSUGold2 reproduces the PREX result but grossly overestimates the neutron skin thickness reported by both CREX and RIKEN. We note that the strong correlation displayed in Fig.3 extends to other set of functionals—both of relativistic and non-relativistic nature—especially in the case of  $^{132}\text{Sn}$ ; see Fig.2 in Ref. [52].

Whereas Fig.3 provides insights into the systematic uncertainties among models that successfully reproduce ground-state observables, Fig.4 quantifies the statistical uncertainties within each individual model. Displayed in Fig.4 are the correlations between the neutron skin thickness of  $^{208}\text{Pb}$ ,  $^{132}\text{Sn}$ , and  $^{48}\text{Ca}$  as predicted by the covariance analysis of both FSUGarnet and FSUGold2. The figure highlights the robust nature of these correlations: within a given theoretical framework, the predictions for these three doubly magic nuclei display—as in the case of Fig.3—nearly perfect correlation coefficients. We observe that while the CREX-like FSUGarnet aligns with the thinner skins reported by CREX and the RIKEN measurement, its prediction for  $^{208}\text{Pb}$  falls significantly short of the PREX result. Conversely, FSUGold2 accurately captures the thick neutron skin of  $^{208}\text{Pb}$  but overestimates the neutron skins of both  $^{48}\text{Ca}$  and  $^{132}\text{Sn}$  by a fairly wide margin.

In summary, the combined constraints from  $^{48}\text{Ca}$ ,  $^{132}\text{Sn}$ , and  $^{208}\text{Pb}$  define a particularly stringent test for modern nuclear theory. Like CREX, the recent measurement of the matter radius of  $^{132}\text{Sn}$  appears to favor a relatively soft symmetry energy, thereby sharpening the tension with the PREX result for  $^{208}\text{Pb}$ . Reconciling the neutron skins of these three doubly magic nuclei within a unified theoretical framework

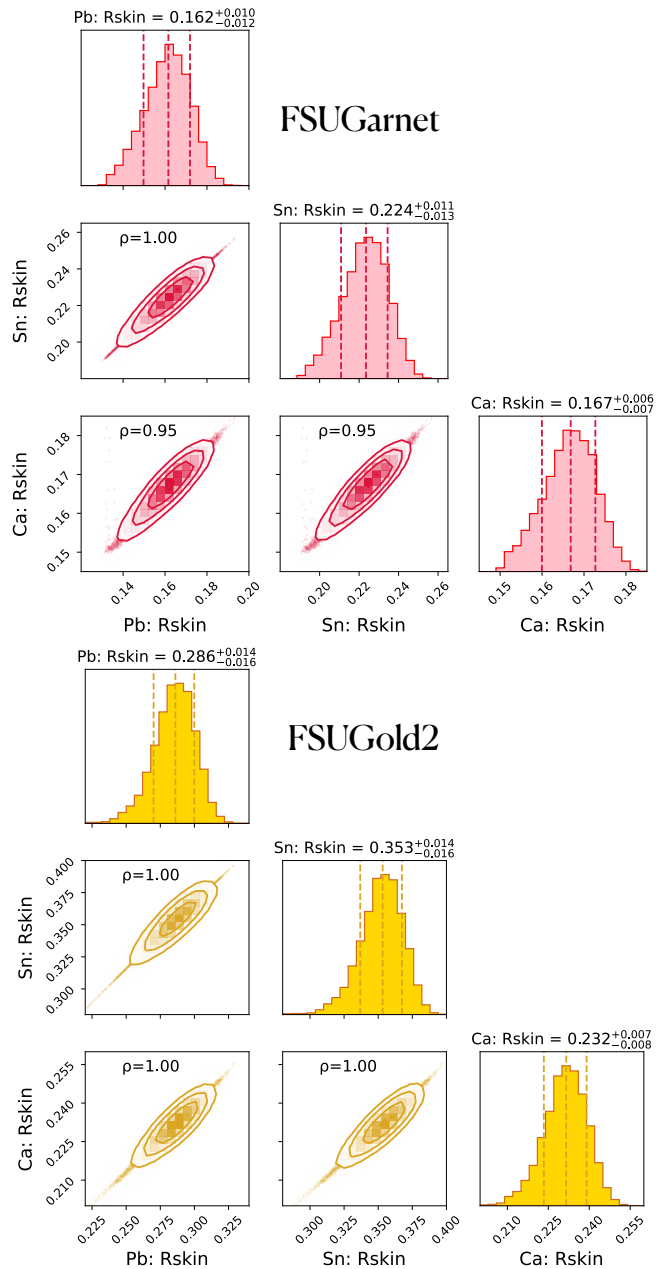


FIG. 4. Statistical correlations between neutron skin thicknesses obtained from the covariance analysis of the FSUGarnet and FSUGold2 energy density functionals. The neutron skins of  $^{208}\text{Pb}$ ,  $^{132}\text{Sn}$ , and  $^{48}\text{Ca}$  exhibit nearly perfect correlations, underscoring the difficulty of simultaneously reproducing all experimental constraints within a single model.

thus remains an outstanding challenge that signals the need for an improved description of the isovector sector of nuclear energy density functionals and possibly of the underlying nuclear forces. In this regard, an independent confirmation of the PREX result—such as that anticipated from the proposed Mainz Radius EXperiment (MREX) at the MESA facility—will be critically important [53].

- [1] A. W. Steiner, M. Prakash, J. M. Lattimer, and P. J. Ellis, Isospin asymmetry in nuclei and neutron stars, *Phys. Rept.* **411**, 325 (2005).
- [2] M. Tsang, J. Stone, F. Camera, P. Danielewicz, S. Gandolfi, et al., Constraints on the symmetry energy and neutron skins from experiments and theory, *Phys. Rev.* **C86**, 015803 (2012).
- [3] C. J. Horowitz, E. F. Brown, Y. Kim, W. G. Lynch, R. Michaels, et al., A way forward in the study of the symmetry energy: experiment, theory, and observation, *J. Phys.* **G41**, 093001 (2014).
- [4] M. Baldo and G. F. Burgio, The nuclear symmetry energy, *Progress in Particle and Nuclear Physics* **91**, 203 (2016).
- [5] B.-A. Li, Progress in constraining nuclear symmetry energy using astrophysical observations, *Universe* **7**, 182 (2021).
- [6] S. Abrahamyan, Z. Ahmed, H. Albatineh, K. Aniol, D. S. Armstrong, et al., Measurement of the Neutron Radius of  $^{208}\text{Pb}$  Through Parity-Violation in Electron Scattering, *Phys. Rev. Lett.* **108**, 112502 (2012).
- [7] C. J. Horowitz, Z. Ahmed, C. M. Jen, A. Rakhman, P. A. Souder, et al., Weak charge form factor and radius of  $^{208}\text{Pb}$  through parity violation in electron scattering, *Phys. Rev.* **C85**, 032501 (2012).
- [8] D. Adhikari et al. (PREX), Accurate Determination of the Neutron Skin Thickness of  $^{208}\text{Pb}$  through Parity-Violation in Electron Scattering, *Phys. Rev. Lett.* **126**, 172502 (2021).
- [9] D. Adhikari et al. (CREX), Precision Determination of the Neutral Weak Form Factor of  $^{48}\text{Ca}$ , *Phys. Rev. Lett.* **129**, 042501 (2022).
- [10] B. T. Reed, F. J. Fattoyev, C. J. Horowitz, and J. Piekarewicz, Implications of PREX-II on the equation of state of neutron-rich matter, *Phys. Rev. Lett.* **126**, 172503 (2021).
- [11] B. Hu et al., Ab initio predictions link the neutron skin of  $^{208}\text{Pb}$  to nuclear forces, *Nature Phys.* **18**, 1196 (2022).
- [12] P.-G. Reinhard, X. Roca-Maza, and W. Nazarewicz, Combined Theoretical Analysis of the Parity-Violating Asymmetry for  $^{48}\text{Ca}$  and  $^{208}\text{Pb}$ , *Phys. Rev. Lett.* **129**, 232501 (2022).
- [13] Z. Zhang and L.-W. Chen, Bayesian Inference of the Symmetry Energy and the Neutron Skin in  $^{48}\text{Ca}$  and  $^{208}\text{Pb}$  from CREX and PREX-2, (2022), arXiv:2207.03328 [nucl-th].
- [14] C. Mondal and F. Gulminelli, Nucleonic metamodelling in light of multimessenger, PREX-II, and CREX data, *Phys. Rev. C* **107**, 015801 (2023).
- [15] P. Papakonstantinou, Nuclear symmetry energy and the PREX-CREX neutron skin puzzle within the KIDS framework (2022) arXiv:2210.02696 [nucl-th].
- [16] E. Yüksel and N. Paar, Implications of parity-violating electron scattering experiments on  $^{48}\text{Ca}$  (CREX) and  $^{208}\text{Pb}$  (PREX-II) for nuclear energy density functionals, *Phys. Lett. B* **836**, 137622 (2023).
- [17] F. Li, B.-J. Cai, Y. Zhou, W.-Z. Jiang, and L.-W. Chen, Effects of Isoscalar- and Isovector-scalar Meson Mixing on Neutron Star Structure, *Astrophys. J.* **929**, 183 (2022).
- [18] V. Thakur, R. Kumar, P. Kumar, V. Kumar, M. Kumar, C. Mondal, B. K. Agrawal, and S. K. Dhiman, Effects of an isovector scalar meson on the equation of state of dense matter within a relativistic mean field model, *Phys. Rev. C* **106**, 045806 (2022).
- [19] T. Miyatsu, M.-K. Cheoun, K. Kim, and K. Saito, Can the PREX-2 and CREX results be understood by relativistic mean-field models with the astrophysical constraints?, *Phys. Lett. B* **843**, 138013 (2023).
- [20] B. T. Reed, F. J. Fattoyev, C. J. Horowitz, and J. Piekarewicz, Density dependence of the symmetry energy in the post-PREX-CREX era, *Phys. Rev. C* **109**, 035803 (2024).
- [21] F. Sammarruca, The Neutron Skin of  $^{48}\text{Ca}$  and  $^{208}\text{Pb}$ : A Critical Analysis, *Symmetry* **16**, 34 (2024).
- [22] M. Salinas and J. Piekarewicz, Impact of tensor couplings with scalar mixing on covariant energy density functionals, *Phys. Rev. C* **109**, 045807 (2024).
- [23] T.-G. Yue, Z. Zhang, and L.-W. Chen, PREX and CREX: Evidence for Strong Isovector Spin-Orbit Interaction, (2024), arXiv:2406.03844 [nucl-th].
- [24] T. Zhao, Z. Lin, B. Kumar, A. W. Steiner, and M. Prakash, Characterizing the nuclear models informed by PREX and CREX: a view from Bayesian inference, (2024), arXiv:2406.05267 [nucl-th].
- [25] X. Roca-Maza and D. H. Jakubassa-Amundsen, QED corrections to the parity-violating asymmetry in high-energy electron-nucleus collisions, (2025), arXiv:2501.14375 [nucl-th].
- [26] A. Kunjipurayil, J. Piekarewicz, and M. Salinas, Role of the isovector spin-orbit potential in mitigating the CREX-PREX dilemma, *Phys. Rev. C* **112**, 014310 (2025).
- [27] Y. Hijikata et al., First Extraction of the Matter Radius of  $^{132}\text{Sn}$  via Proton Elastic Scattering at 200 MeV/Nucleon, *PTEP* **2026**, 013D02 (2026), arXiv:2602.08455 [nucl-ex].
- [28] C. Gorges et al., Laser spectroscopy of neutron-rich tin isotopes: A discontinuity in charge radii across the  $N = 82$  shell closure, *Phys. Rev. Lett.* **122**, 192502 (2019).
- [29] F. P. Gustafsson et al., Charge Radii Measurements of Exotic Tin Isotopes in the Proximity of  $N=50$  and  $N=82$ , *Phys. Rev. Lett.* **135**, 222501 (2025).
- [30] P. Arthuis, C. Barbieri, M. Vorabbi, and P. Finelli, *AbInitio* Computation of Charge Densities for Sn and Xe Isotopes, *Phys. Rev. Lett.* **125**, 182501 (2020).
- [31] P. Adrich et al., Evidence for pygmy and giant dipole resonances in  $^{130}\text{Sn}$  and  $^{132}\text{Sn}$ , *Phys. Rev. Lett.* **95**, 132501 (2005).
- [32] J. Piekarewicz, Pygmy dipole resonance as a constraint on the neutron skin of heavy nuclei, *Phys. Rev.* **C73**, 044325 (2006).
- [33] A. Klimkiewicz et al., Nuclear symmetry energy and neutron skins derived from pygmy dipole resonances, *Phys. Rev.* **C76**, 051603 (2007).
- [34] N. Paar, D. Vretenar, E. Khan, and G. Colò, Exotic modes of excitation in atomic nuclei far from stability, *Rept. Prog. Phys.* **70**, 691 (2007).
- [35] J. Piekarewicz, Pygmy Resonances and Neutron Skins, *Phys. Rev.* **C83**, 034319 (2011).
- [36] A. Carbone, G. Colò, A. Bracco, L.-G. Cao, P. F. Bortignon, et al., Constraints on the symmetry energy and on neutron skins from the pygmy resonances in  $^{68}\text{Ni}$  and  $^{132}\text{Sn}$ , *Phys. Rev.* **C81**, 041301 (2010).
- [37] D. Savran, T. Aumann, and A. Zilges, Experimental studies of the Pygmy Dipole Resonance, *Prog. Part. Nucl. Phys.* **70**, 210 (2013).
- [38] F. Le Blanc et al., Charge-radius change and nuclear moments in the heavy tin isotopes from laser spectroscopy: Charge radius of  $^{132}\text{Sn}$ , *Phys. Rev. C* **72**, 034305 (2005).
- [39] K. L. Jones et al., The magic nature of  $^{132}\text{Sn}$  explored through the single-particle states of  $^{133}\text{Sn}$ , *Nature* **465**, 454 (2010).
- [40] V. Vaquero et al., Fragmentation of Single-Particle Strength around the Doubly Magic Nucleus  $^{132}\text{Sn}$  and the Position of the  $0f_{5/2}$  Proton-Hole State in  $^{131}\text{In}$ , *Phys. Rev. Lett.* **124**, 022501 (2020).
- [41] K. L. Jones et al., Direct reaction measurements with a  $^{132}\text{Sn}$  radioactive ion beam, *Phys. Rev. C* **84**, 034601 (2011).

- [42] C. J. Horowitz and J. Piekarewicz, Neutron star structure and the neutron radius of  $^{208}\text{Pb}$ , Phys. Rev. Lett. **86**, 5647 (2001).
- [43] F. J. Fattoyev, C. J. Horowitz, J. Piekarewicz, and G. Shen, Relativistic effective interaction for nuclei, giant resonances, and neutron stars, Phys. Rev. **C82**, 055803 (2010).
- [44] W.-C. Chen and J. Piekarewicz, Building relativistic mean field models for finite nuclei and neutron stars, Phys. Rev. **C90**, 044305 (2014).
- [45] W.-C. Chen and J. Piekarewicz, Searching for isovector signatures in the neutron-rich oxygen and calcium isotopes, Phys. Lett. **B748**, 284 (2015).
- [46] B. A. Brown, Neutron radii in nuclei and the neutron equation of state, Phys. Rev. Lett. **85**, 5296 (2000).
- [47] R. J. Furnstahl, Neutron radii in mean-field models, Nucl. Phys. **A706**, 85 (2002).
- [48] X. Roca-Maza, M. Centelles, X. Viñas, and M. Warda, Neutron skin of  $^{208}\text{Pb}$ , nuclear symmetry energy, and the parity radius experiment, Phys. Rev. Lett. **106**, 252501 (2011).
- [49] D. W. Sprung and J. Martorell, The symmetrized Fermi function and its transforms, J. Phys. A **30**, 6525 (1997).
- [50] J. Piekarewicz, A. R. Linero, P. Giuliani, and E. Chicken, Power of two: Assessing the impact of a second measurement of the weak-charge form factor of  $^{208}\text{Pb}$ , Phys. Rev. **C94**, 034316 (2016).
- [51] J. Piekarewicz and S. Weppner, Insensitivity of the elastic proton-nucleus reaction to the neutron radius of Pb-208, Nucl.Phys. **A778**, 10 (2006), arXiv:nucl-th/0509019 [nucl-th].
- [52] J. Piekarewicz, B. Agrawal, G. Colò, W. Nazarewicz, N. Paar, et al., Electric dipole polarizability and the neutron skin, Phys. Rev. **C85**, 041302(R) (2012).
- [53] S. Schlimme et al., The MESA physics program, EPJ Web Conf. **303**, 06002 (2024).

#### ACKNOWLEDGMENTS

The author is grateful to Profs. K. Kemper and M. Spieker for useful discussions. This material is based upon work supported by the U.S. Department of Energy Office of Science, Office of Nuclear Physics under Award Numbers DE-FG02-92ER40750 and DE-SC0009883.